ACS Catalysis

Perspective

Cite This: ACS Catal. 2018, 8, 770−784

pubs.acs.org/acscatalysis

Consideration of the Aluminum Distribution in Zeolites in Theoretical and Experimental Catalysis Research

Brandon C. Knott,[†,¶] Claire T. Nimlos,[‡,¶] David J. Robichaud,[†] Mark R. Nimlos,[§] Seonah Kim,[*,§] and Rajamani Gounder[*,‡]

[†]Biosciences Center, National Renewable Energy Laboratory, 15013 Denver West Parkway, Golden, Colorado 80401-3393, United States

[‡]Charles D. Davidson School of Chemical Engineering, Purdue University, 480 Stadium Mall Drive, West Lafayette, Indiana 47907, United States

[§]National Bioenergy Center, National Renewable Energy Laboratory, 15013 Denver West Parkway, Golden, Colorado 80401-3393, United States

ABSTRACT: Research efforts in zeolite catalysis have become increasingly cognizant of the diversity in structure and function resulting from the distribution of framework aluminum atoms, through emerging reports of catalytic phenomena that fall outside those recognizable as the shape-selective ones emblematic of its earlier history. Molecular-level descriptions of how active-site distributions affect catalysis are an aspirational goal articulated frequently in experimental and theoretical research, yet they are limited by imprecise knowledge of the structure and behavior of the zeolite materials under interrogation. In experimental research, higher precision can result from more reliable control of structure during synthesis and from more robust and quantitative structural and kinetic characterization probes. In theoretical research, construction of models with specific aluminum locations and distributions seldom capture the heterogeneity inherent to the materials studied by experiment. In this Perspective, we discuss research findings that appropriately frame the challenges in developing more predictive synthesis−structure−function relations for zeolites, highlighting studies on ZSM-5 zeolites that are among the most structurally complex molecular sieve frameworks and the most widely studied because of their versatility in commercial applications. We discuss research directions to address these challenges and forge stronger connections between zeolite structure, composition, and active sites to catalytic function. Such connections promise to aid in bridging the findings of theoretical and experimental catalysis research, and transforming zeolite active site design from an empirical endeavor into a more predictable science founded on validated models.

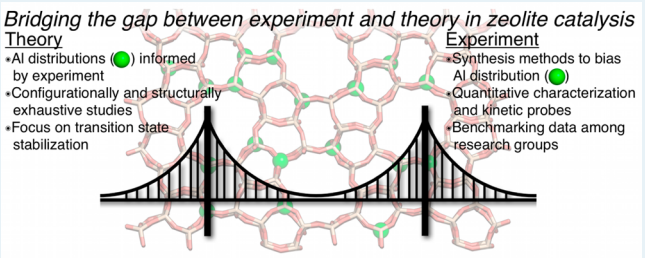

KEYWORDS: *zeolite, aluminum distribution, confinement, computational catalysis, ZSM-5*

Zeolites are ubiquitous as solid acid catalysts, notably in the conversion and refining of petroleum-derived hydrocarbons to chemical and fuel products[1] and as shape-selective molecular sieves that regulate catalytic reactivity through size-exclusion principles.[2] In the late 1960s, zeolites replaced amorphous silica−alumina catalysts to revolutionize fluid catalytic cracking processes in refineries that produce gasoline,[3] and they have since been used in several other shape-selective applications.[2] Specifically, aluminum-substituted MFI zeolites (ZSM-5) are used in a variety of hydrocarbon upgrading processes, including the oligomerization of light olefins to form gasoline and distillate,[4,5] and in upgrading methanol to olefins, gasoline, and hydrocarbons (MTO, MTG, MTH).[6] ZSM-5 zeolites have also been explored as catalysts to produce chemicals and fuels from alternate carbon feedstocks such as renewable lignocellulosic biomass sources,[7] especially within thermochemical conversion schemes,[8] and light hydrocarbons in shale gas.[9] Additionally, metal-exchanged zeolites (e.g., Cu-ZSM-5, Cu-SSZ-13) provide different functionality and reactivity, as in the partial oxidation of methane to methanol,[10] selective reduction of nitrogen oxides in emissions control,[11] and homologation of biomass-derived oxygenates to transportation fuels.[12]

Experimental and theoretical studies focused on catalysis by zeolites continue to expand in breadth and scope, motivating higher levels of resolution and detail about the synthesis and characterization of these materials and the construction of models that describe their structure and properties. Structural features at several length scales influence zeolite reactivity, and we refer the reader to effects at the mesoscale and macroscale in other review articles,[13−16] which are beyond the scope of this Perspective. Here, we focus on molecular and atomic length scales (i.e., sub-nanometer) that define the structure and

Received: October 26, 2017
Revised: December 6, 2017
Published: December 11, 2017

DOI: 10.1021/acscatal.7b03676
ACS Catal. 2018, 8, 770−784

behavior of active sites and the chemical reactions they mediate and inform the construction of models to describe active sites and reaction coordinates. When considering the structure of framework Al atoms, model construction requires, at the very least, knowledge or assumptions of the following: (i) the bulk elemental composition (the Si/Al ratio, or number of Al atoms per unit cell), (ii) the lattice positions of the Al atoms (their distribution among crystallographically unique lattice sites), and (iii) the relative proximity of lattice Al atoms (the distribution of interatomic Al−Al distances among framework Al-site pairs). Further knowledge is needed to define the structure of the attendant protons (H^+) or exchanged metal complexes that serve as catalytic active sites and their location at the four bridging oxygen atoms at each Al center that bear anionic charges. This definition is further complicated upon equilibration among different O-site locations under reaction conditions, which determines the void spaces within which active sites are contained.

In this Perspective, we summarize recent experimental progress toward developing synthesis methods to bias, and characterization methods to identify, the crystallographic locations and arrangements of Al substituted within zeolite frameworks. We focus on MFI because it is among the lowest symmetry molecular sieve frameworks and thus captures many of the challenges introduced by structural complexity, and because it is ubiquitous in industrial practice and thus among the most widely studied frameworks. We note that more comprehensive reviews on this topic can be found elsewhere,[17] and we focus the discussion here on how computational studies have complemented experimental efforts to bias and characterize framework Al siting. In doing so, we highlight the implications of Al distribution in zeolites for constructing accurate structural models in theoretical studies of catalytic phenomena (e.g., density functional theory (DFT) calculations), focusing on MFI while making connections to other zeolites as appropriate. In reviewing computational studies, we discuss the motivating factors underlying the choices in model construction. We conclude with an outlook that highlights advances in experiment and theory that would provide further clarity into framework Al arrangements in zeolites and their effects on catalysis.

2. THE MFI CRYSTAL STRUCTURE

The MFI structure comprises pentasil building units, which consist of eight five-membered rings (5-MR) that combine to form pentasil chains. The resulting framework contains straight and sinusoidal 10-MR channels that intersect to form larger cavities. Figure 1 shows the MFI structure oriented to view down the central *b*-axis of the 10-MR straight channels, in which 5-MR, 6-MR, and 10-MR are discernible.[18−20] MFI belongs to the class of medium-pore zeolites, which are materials containing 10-MR as the largest micropores.[21] The total micropore volume of MFI comprises 45% of its total crystal volume; of this pore volume, 53% (24% of total) is contained within 10-MR channels and 26% (12% of total) is contained within larger channel intersection voids (i.e., cages).[22] The pore-limiting diameter (PLD) is 5.0 Å, which corresponds to the characteristic size of the largest guest molecule for which the accessible pore volume is nonzero, while the largest cavity diameter (LCD) is 7.0 Å, which resembles the maximum transition state structure that can be accommodated.

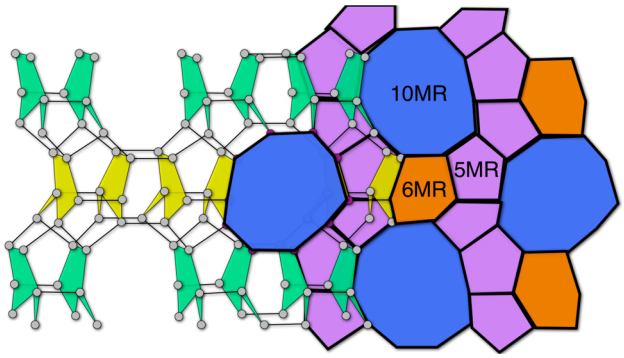

Figure 1. MFI crystal structure (left) shown using ball-and-stick visualization to highlight the pentasil rings in green and yellow in alternating rows and (right) shown with color-coded shades by ring size to highlight the 5-MR (purple), 6-MR (orange), and 10-MR (blue) created by the pentasil building blocks.

Zeolite frameworks are composed of tetrahedral sites (T-sites) occupied by silicon atoms that are linked through a bridging oxygen atom. When a silicon atom is replaced with aluminum, a negative charge is imparted to the zeolite framework and shared among the four bridging oxygen atoms, and it is counterbalanced by a Brønsted acidic proton or an extra-lattice cationic site or complex. The orthorhombic form of MFI contains 12 crystallographically distinct T-sites and is the more thermodynamically stable form above 340 K. The monoclinic form of MFI contains 24 distinct T-sites and is most stable below this transition temperature;[23] however, the monoclinic-to-orthorhombic symmetry transformation can be induced by the adsorption of small molecules (e.g., *p*-xylene) at ambient temperatures.[18] When this phase transition occurs, the symmetry plane (*m* in Figure 2) is broken. As shown in Figure 2, the 24 T-sites of the monoclinic form correspond to the 12 T-sites of the orthorhombic form. This correspondence among T-sites can be helpful in understanding framework Al locations in ZSM-5, as some studies focus on the monoclinic form.[24,25] The T1, T2, T3, T5, T6, T7, T9, and T12 sites are accessible within channel intersections, while T4 and T10 are within the sinusoidal channel and T8 and T11 are within the straight channel.[26]

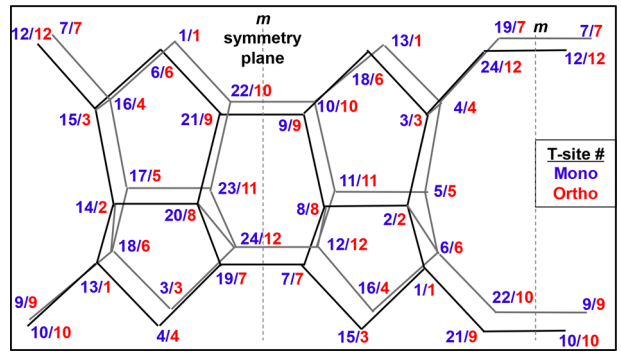

Figure 2. Orthorhombic and monoclinic forms of ZSM-5. The lattice T-sites for the orthorhombic form are shown in red; those for the monoclinic form are shown in blue. Figure adapted with permission from van Koningsveld et al.[23] Copyright 1990 Elsevier.

DOI: 10.1021/acscatal.7b03676
ACS Catal. 2018, 8, 770−784

3. EARLY HISTORY OF ZSM-5: A "SINGLE-SITE" CATALYST

ZSM-5 was first prepared in synthetic laboratories in the 1960s, and patented by the Mobil Oil Corporation in 1972.[27] Kerr used tetraalkylammonium ions to show that zeolites could be synthesized through a structure directing agent (SDA)-assisted synthesis,[28] which was subsequently used by Landolt and Argauer in 1965 to synthesize ZSM-5.[27] Compared with other commercially used zeolites and Brønsted acid catalysts, ZSM-5 showed higher adsorption rates of linear alkanes and lower amounts of coke formation, which were beneficial properties for alkane hydrocracking to produce diesel and heavier fuels.[29] By measuring differences in the cracking and adsorption rates of different hexane isomers, Chen and Garwood reported that MFI micropores could discriminate among linear and branched alkane reactants in cracking reactions and thus influence catalysis via reactant shape selectivity phenomena.[30] Following these original reports, ZSM-5 zeolites were applied to a wider range of industrially practiced reactions and reported to influence catalysis via other shape selective phenomena, including transition state shape selectivity and product shape selectivity during xylene isomerization and toluene disproportionation, respectively.[31−33]

In addition to hydrocarbon processing and refining, the search for alternate carbon feedstocks for fuel and chemical production motivated efforts to upgrade renewable biomass through catalytic processes using ZSM-5 zeolites. In 1986, Chen and colleagues demonstrated that ZSM-5 could convert biomass-derived carbohydrates to hydrocarbons, with coke, CO, and CO_2 as the major byproducts.[34] One challenge in biomass conversion is to remove sufficient oxygen to produce fuels and chemicals of comparable composition and structure to those synthesized from petroleum sources.[34] ZSM-5 has been routinely studied in biomass conversion routes because of its hydrothermal stability and mitigated coke formation, compared with zeolites with smaller or larger pore sizes, when reacting biomass model compounds and biomass-derived feeds.[35−39] These examples reflect the advent of ZSM-5 as a versatile medium-pore zeolite that had a large impact on catalytic applications driven by shape selective phenomena.

In a seminal contribution to the field of zeolite catalysis, Haag and co-workers studied the physicochemical and catalytic properties of a series of ZSM-5 samples prepared with a wide range of Al content (Si/Al = 10−10 000).[40] Catalytic properties were probed using the alpha test, which compares the rate of *n*-hexane cracking measured on a solid acid relative to that measured on amorphous silica−alumina. The alpha test value[41] (per volume) increased linearly with the total Al content (ppm) among these ZSM-5 zeolites (Figure 3),[40] along with cesium ion uptakes and water uptakes from adsorption experiments.[42] From these observations, the authors concluded that protons compensating each Al site were catalytically equivalent, despite the diversity of T-sites present in the MFI framework. These results may also indicate that the alpha test reaction is insensitive to protons located at different Al T-sites or that the methods used to prepare these samples crystallized ZSM-5 with similar Al distributions among different T-sites, as the authors also hypothesized. Regardless of the underlying reasons for the observation reported in Figure 3, this report provided visionary guidance that a given zeolite framework could behave as an ideal single-site heterogeneous catalyst.[43]

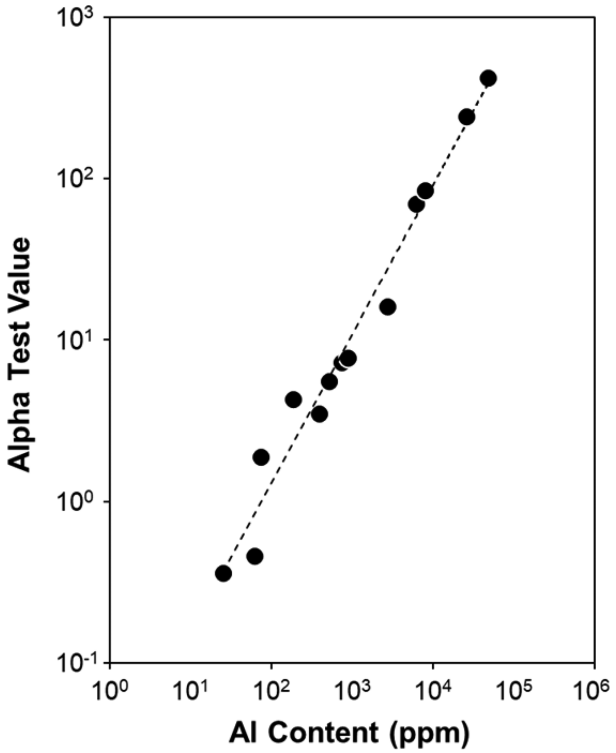

Figure 3. Cracking rates of *n*-hexane on ZSM-5 zeolites of varying bulk Al content. Alpha test values (811 K). Figure adapted with permission from Haag et al.[40] Copyright 1984 Macmillan Publishers Limited.

4. AL LOCATION AT DIFFERENT T-SITES AND CONSEQUENCES OF CONFINEMENT

The collective experimental work discussed in Section 3 supported the viewpoint that aluminosilicate zeolites predominantly influence catalysis by imposing shape selective control through their pore architecture and that the proton active sites compensating framework Al atoms behave similarly for Brønsted acid-catalyzed reactions. At first glance, this proposal seems consistent with the essentially invariant Brønsted acid strength of OH groups compensating framework Al atoms at different zeolitic T-sites, as assessed by periodic DFT estimates of the deprotonation energy (a probe-independent measure of Brønsted acid strength) when rigorously ensemble-averaged among OH groups at the four bridging oxygen atoms at each Al T-site.[44] Yet, acid sites located within different voids of a zeolite, because of the specific Al T-sites they compensate, can behave catalytically different due to confinement effects and differences in van der Waals stabilization of the relevant reactive intermediates and transition states.[45,46]

4.1. Catalysis. Catalytic probe reactions have been used to make inferences about Al siting and thus proton location in ZSM-5. The constraint index (CI) test, given by the *n*-hexane-to-3-methylpentane cracking rate ratio (673 K, 40 kPa alkane), has been used to probe the void size around acid sites because smaller pores generally correlate with higher constraint index values, although anomalous results are observed in certain cases.[47] Yokoi et al. have reported how different synthesis routes to crystallize ZSM-5 samples lead to different Al distributions among smaller straight and sinusoidal channels

DOI: 10.1021/acscatal.7b03676
ACS Catal. 2018, 8, 770−784

(PLD = ∼ 5 Å) and larger-channel intersections (LCD = ∼ 7 Å), assessed from corresponding changes in CI values.[48,49] Janda and Bell have used *n*-alkane cracking and dehydrogenation to report that dehydrogenation is preferred over cracking on protons located within larger channel intersections of ZSM-5, which are proposed to preferentially stabilize later and looser *n*-alkane dehydrogenation transition states.[50]

The product distributions resulting from catalytic conversion of methanol to olefins have also been used to infer the location of protons within different confining void environments, as larger voids generally favor intermediates in aromatic-based cycles and smaller voids generally favor reactive intermediates in olefin-based cycles. This approach was used to study ZSM-5 zeolites synthesized using different silicon precursors, which resulted in different Al distributions between channels and intersections[51] as characterized by ^{27}Al MAS NMR spectra and UV−vis spectra after cobalt exchange. Product distributions from MTO were similar to those expected from the aromatic-based cycle (enriched in ethene and aromatics) in ZSM-5 samples with acid sites located predominantly in larger channel intersections (LCD = ∼ 7 Å), but included more products of the olefin-based cycle (enriched in propene and higher olefins) in samples with acid sites distributed among intersections and smaller channels (PLD = ∼ 5 Å). Similar studies of MCM-22 zeolites reported that the addition of boron to synthesis media influenced the location of Al within the frameworks of crystallized products.[52] In combination with a theoretical study,[53] acid sites in smaller sinusoidal channels of MCM-22 were found to favor the olefin-based cycle, while acid sites in larger supercages and surface pockets were found to favor the aromatic-based cycle. These studies of MTO catalysis further demonstrate how the location of acid sites in different confining environments can influence catalytic behavior.

Methanol dehydration to dimethyl ether is a more precise and quantitative probe reaction of acid strength and confinement effects in zeolites,[54] because first-order and zero-order rate constants show different sensitivity to these effects and have been calibrated on a variety of solid acids of well-defined structure and composition.[55−57] The first-order dehydration rate constant is sensitive to both the confining environment around and the strength of the acid site, because kinetically relevant dimethyl ether formation transition states and adsorbed methanol monomer species differ in their size and charge, respectively.[54] The zero-order dehydration rate constant is sensitive primarily to acid strength, because the kinetically relevant transition state and the coadsorbed methanol dimer are similar in size but not in charge.[54] Thus, analysis of both rate constants can be used to distinguish among acid sites within different confining environments of the same zeolite topology, and it can determine whether different Al locations influence acid site strength, which has been studied computationally.[58]

Jones et al. measured first-order and zero-order methanol dehydration rate constants on a series of commercial ZSM-5 samples of varying Si/Al ratio (17−118), and incidentally different framework Al distributions, as shown in Figure 4.[55] Zero-order rate constants (433 K) were similar among all samples, consistent with similar acid strength for protons among different Al T-site locations in zeolites, as also observed by theory.[44] First-order rate constants were measured at values expected for void sizes characteristic of channel intersections (LCD = ∼ 7 Å) and invariant with Al content among most ZSM-5 samples, yet they were higher on the ZSM-5 sample

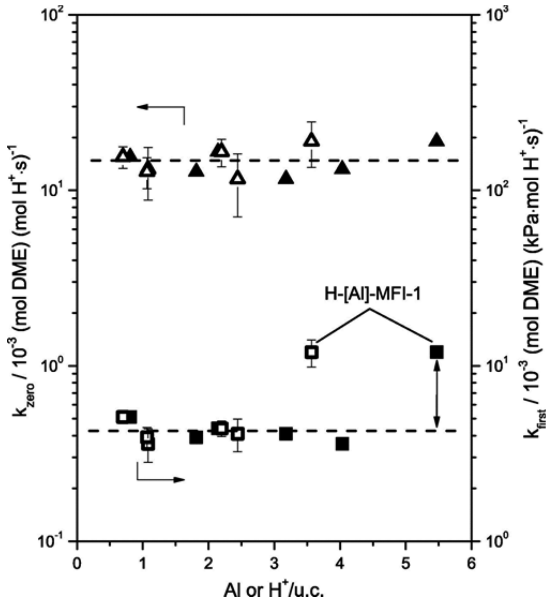

Figure 4. Zero-order and first-order rate constants (433 K) for methanol dehydration on commercial ZSM-5 samples with widely varying Al (closed) and H^+ (open) contents. Figure reproduced with permission from Jones et al.[55] Copyright 2011 Elsevier.

with the highest Al content. This data point (H-[Al]-MFI-1; Figure 4) suggested the preferential positioning of protons (of equivalent acid strength) within more constrained (PLD = ∼ 5 Å) 10-MR-channel locations at such high Al densities. These studies demonstrate the insight into Al location that is possible when using quantitative probes, even within complex molecular sieve frameworks such as MFI.

4.2. Characterization. The recognition that proton active sites within a given zeolite can show different catalytic behavior motivates the development of structural characterization methods that distinguish protons among different void environments and Al atoms among different T-sites. Direct characterization of Al atoms typically relies on ^{27}Al magic angle spinning nuclear magnetic resonance (MAS NMR), used routinely to distinguish between tetrahedrally coordinated Al in framework positions and octahedrally coordinated Al in extra-framework locations.

Sklenak et al. prepared 11 monoclinic ZSM-5 samples using different synthesis protocols (Si/Al = 14−45), measured different envelopes for tetrahedral resonances in their ^{27}Al multiple quantum (MQ) MAS NMR spectra, and used hybrid quantum mechanics/molecular mechanics (QM/MM) calculations to predict ^{27}Al chemical shifts at different T-site locations to assign resonances to specific locations.[59] This same approach was used later to study Al location in ferrierite zeolites.[60] Several MFI T-sites were characterized by ^{27}Al chemical shifts too similar to be distinguished by experiment and thus allowed for only partial assignment of Al substitution patterns among different T-sites. The authors concluded that T1, T4, T6, T7, T8, and T12 sites were substituted by Al among the samples examined, but that any given sample had no more than 3−4 different T-sites occupied by Al. In a subsequent study, Sklenak et al. reported seven additional synthesis conditions that resulted in ZSM-5 samples with Si/Al ratios up to 140,[25] which revealed two new ^{27}Al NMR resonances that were assigned to T20 and T24. Notably, Al substitution at five different T-sites was detected even for

DOI: 10.1021/acscatal.7b03676
ACS Catal. 2018, 8, 770−784

samples containing dilute Al contents corresponding to less than one per unit cell (Si/Al = 140), suggesting either weak thermodynamic preferences for Al siting at a particular T-site or that thermodynamic considerations do not influence Al siting during crystallization.

In recent years, Yokoi et al. have used a high-resolution ^{27}Al MAS NMR technique proposed to distinguish between Al located in larger void intersections.[48,49,61] Lower-resolution ^{27}Al MAS NMR is unable to characterize different Al species because of quadrupolar Al interactions that cause resonance broadening; however, high sample spin rates and large quantities of accumulated scans, together with ^{27}Al MQ MAS NMR were used to assign five distinct peaks for Al species (Figure 5). Specifically, the ^{27}Al resonances at 54 and

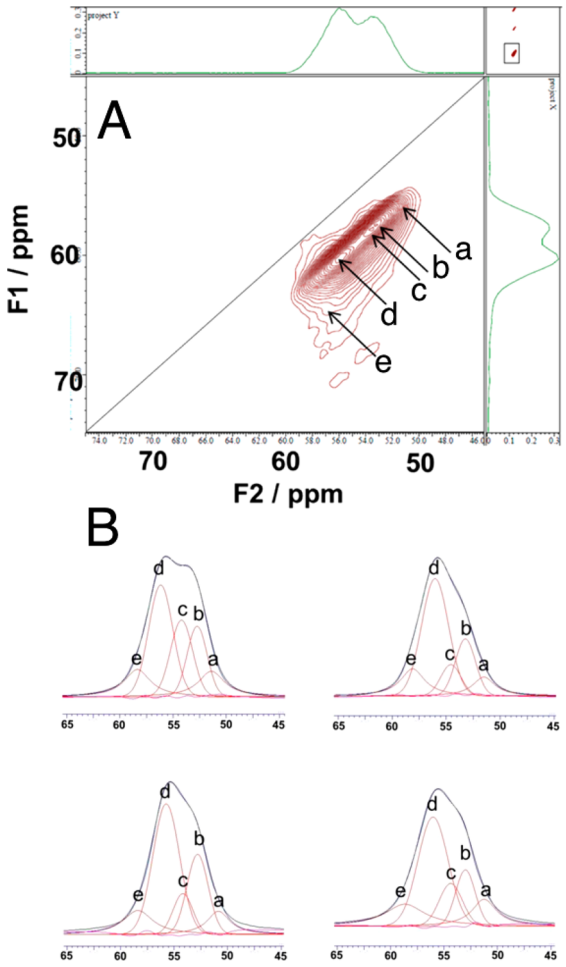

Figure 5. MQ MAS NMR peak assignments (a−e) for different T-sites in ZSM-5 (A) used to deconvolute high resolution one-dimensional MAS NMR (B) for assignment of Al in different locations in ZSM-5. Figure reproduced with permission from Yokoi et al.[49] Copyright 2015 American Chemical Society.

56 ppm are proposed to correspond to the channel intersection and to the straight and/or sinusoidal channel locations, respectively.[48,49,61]

Recent studies of Beta zeolite have used Al K-edge X-ray adsorption near edge spectroscopy (XANES), as well as extended X-ray adsorption fine structure (EXAFS), to determine Al−O and Al−Si distances up to 3−4 atoms away, in order to obtain quantitative measurements of the Al T-site distribution.[62] In combination with ab initio DFT calculations, Al EXAFS spectra were used to measure Al separated by up to 6 Å and to quantify the amount of Al in framework and extra-framework positions. Al site populations did not follow predictions from thermodynamic stabilities, supporting the hypothesis that Al incorporation during synthesis is influenced by crystallization kinetics and the organic SDA used. The authors also reported that a dealuminated zeolite showed a preferential decrease in Al NMR resonances at the T7 and T2 locations, suggesting that certain sites are more susceptible to dealumination while others (T5, T6), are more resistant to Al removal in the Beta structure.[62]

Rietveld refinement of powder X-ray diffraction (XRD) patterns has been used to locate organic SDA molecules occluded within zeolitic void spaces after crystallization, as demonstrated in the case of FER zeolites crystallized using tetramethylammonium (TMA) and pyrrolidine (Pyr).[63] Structural refinement was also used to determine the distances between the carbon and nitrogen atoms in the occluded SDAs and the framework oxygen atoms of the zeolite lattice, in order to assess the strength of interactions between each SDA and the crystalline framework. Positively charged nitrogen centers in Pyr were located closer to their respective framework oxygens than were nitrogen centers in TMA, due to partial shielding by their methyl groups, suggesting that the former SDA could more effectively interact with anionic framework oxygens and thus more strongly direct the incorporation of Al atoms into nearby T-sites. Rietveld refinement of XRD patterns of zeolites containing exchanged extra-framework metal sites has also been used to determine preferences for Al siting in different T-sites;[64−71] however, conclusions regarding the preferred T-sites for Al substitution differ, even with the same cation exchange and characterization technique.[66]

Other characterization techniques have also been used to probe Al siting and distribution in zeolites. Fluorescence spectroscopy with standing X-rays has been used on large crystallites of scolecite zeolite, a more symmetric framework than MFI, to identify the occupied crystallographic T-sites with higher resolution than ^{27}Al NMR methods.[72] Bohinc et al. studied FER zeolites synthesized to contain different Al distributions using valence-to-core X-ray emission spectroscopy (XES), and they observed changes to the intensity and position of X-ray emission lines that were correlated to different Al T-site occupancies.[73] Perea et al. employed atom probe tomography (APT) to detect the three-dimensional spatial distribution, with a 1−2 nm resolution, of individual Al, O, and Si atoms in a ZSM-5 crystal,[74] revealing inhomogeneous Al distributions that become even more heterogeneous upon steam treatment. These techniques to probe Al distributions at various length scales are also useful in the development of synthesis−structure and structure−function relations.

4.3. Synthesis. The effects of ZSM-5 synthesis conditions have been studied to understand how the Al location in the crystalline products can be biased. One approach has been to use mixtures of organic and inorganic SDA molecules in the synthesis solution. Yokoi et al. have demonstrated that ZSM-5 zeolites made using tetrapropylammonium (TPA^+) as the only SDA contain acid sites predominantly located at channel intersections, as probed by the CI test and ^{27}Al MAS NMR.[49] The addition of small amounts of Na^+ to the synthesis solution causes a higher fraction of Al to be located in smaller 10-MR channel environments, evident in higher CI test values and

DOI: 10.1021/acscatal.7b03676
ACS Catal. 2018, 8, 770−784

corresponding changes to ^{27}Al NMR spectra. Additionally, the replacement of the cationic organic TPA$^+$ molecule with the neutral organic pentaerythritol molecule as the SDA leads to preferential siting of Al within 10-MR channels, as probed by the CI test and ^{27}Al MQ MAS NMR.[48,49]

Dědeček et al. reported that the type of reagent and precursor compounds used during synthesis affected the Al siting among different T-sites of the crystallized ZSM-5 products.[24] Using ^{27}Al 3Q MAS NMR techniques in conjunction with QM/MM calculations, the effects of different Al and Na sources were investigated. When different Al precursors were used in the synthesis solution, in the presence of only the organic TPA$^+$ cation as the SDA, resonances for Al T-sites in ZSM-5 channel intersection (54.6. 56.0, and 56.4 ppm) accounted for more than 55% of all Al sites. Dědeček et al. reported that the addition of Na$^+$ to the synthesis medium caused Al to incorporate predominantly at T-sites in the channel intersection, in contrast to the findings of Yokoi et al. Different Na$^+$ and Al sources caused detectable changes in the Al distribution among T-sites in the channels and intersections but without any discernible trends. These data sets and their differing interpretations from various research groups provide motivation for continued work to develop new synthesis methods and to clarify the factors governing Al siting in zeolites.

Boron addition to zeolite synthesis media can cause competition with aluminum for incorporation as the framework heteroatom. Recently, a series of ZSM-5 catalysts prepared with varying B/Al ratios was studied to understand the impact of this parameter on Al siting.[75] Structural characterization using ^{27}Al, ^{29}Si, and ^{11}B MAS NMR indicated that the presence of boron in the synthesis gel influenced the ^{27}Al NMR chemical shifts of framework Al atoms, suggesting that Al may occupy different distributions of lattice T-sites. Similar studies of MCM-22 zeolites provided evidence that boron incorporation influenced the acid site distribution among different void locations, which was assessed by selective poisoning of acid sites located in smaller sinusoidal channels but not those in larger supercages and surface pores.[52] These data demonstrate how the addition of a second heteroatom in zeolite synthesis media provides a method to influence the incorporation and siting of Al into framework locations.

The role of the organic SDA on Al siting in zeolites has been studied in a variety of structures, in which "guest-host" interactions between the organic molecule and the framework influence the incorporation of Al.[76,77] One example is the FER structure, in which tetramethylammonium (TMA) was used in combination with a second bulky organic cation such as pyrrolidine (Pyr), hexamethylenimine (HMI),[78] or other amine compounds.[79] As the second organic SDA contained more cyclic carbons (going from Pyr to HMI), Al was found to preferentially site within larger 10-MR FER voids, as determined from analysis of ^{1}H MAS NMR spectra and the CI test. These data reflect how cooperative structure direction of a given zeolite using organic SDAs of different size, which show different preferences for occupying different voids,[63] influence Al location and siting during synthesis.

4.4. Modeling. Early computational studies of ZSM-5 largely focused on intrinsic structural properties of acidic zeolites, including comparing the stability of each T-site,[80] and the stability of Al[80,81] (or Fe[82]) substitution at various T-sites accounting for Lowenstein's rule of avoiding next-nearest-neighbor Al substitution patterns.[83,84] Other studies focused on discriminating the different types of hydroxyl groups present (terminal SiOH and bridging Al−O(H)-Si),[85] their acid strength[80] and how acid strength may be influenced by zeolite geometry,[86] Al substitution,[81,87] and different types of internal silanol pairs.[88] In addition, early interest focused on the adsorption behavior of various small molecules (benzene,[89] toluene,[89] butane,[89] methanol,[90,91] *p*-xylene,[92] CO,[93,94] H_2O,[93] NH_3,[93] ethylene,[95] acetone,[96] methyl ethyl ketone,[96] diethyl ketone[96]) and on elucidating catalytic mechanisms, such as the formation of carbenium ion intermediates from olefins.[97] Germane to all of these calculations are the choices made in constructing a structural model for ZSM-5 and the T-sites for Al substitution.

Typically, early studies utilized ab initio calculations on clusters comprising just 1−3 T-sites,[80,83−86,88,90,93] with a maximum of five T-sites.[81] Semiempirical methods[82,94−97] enabled modeling larger clusters in some cases, up to 20 T-sites.[91] In one of the first "zeolite" calculations, zero T-sites were included and the interactions of small molecules with a single hydroxyl group (sans tetrahedral atom) were calculated and compared with NMR experiments on zeolites.[89] In what might be considered a precursor of the ONIOM method, some early studies embedded the ab initio QM region in a lattice of point charges modeling the zeolitic environment surrounding the active site.[87,90,91,96]

As discussed in Section 2, the orthorhombic form of ZSM-5 contains 12 crystallographically distinct T-sites. The T12 site is the location most frequently chosen for Al substitution in studies of catalytic reactions in ZSM-5,[94,98−107] often attributed to its accessibility at the intersection of straight and sinusoidal channels.[108−123] As articulated by Ghorbanpour et al., however, two-thirds of the T-sites are also accessible at this intersection and only four T-sites are *not* at the channel intersection.[26] Other studies have indeed chosen different T-sites for Al substitution for the same stated reason.[87,90,119]

The frequent choice of the T12 site for Al substitution may also have resulted from the influential and oft-cited study by Lonsinger et al., wherein this site was determined to be the most thermodynamically stable location for Al substitution via semiempirical molecular orbital calculations of pentameric clusters (5T clusters).[124] Fripiat and co-workers[80,81] concluded that T2 and T12 were most favorable for Al substitution, but they did not attempt to include any effect of the zeolite environment beyond the small clusters treated with ab initio QM, nor did they allow for local structural relaxation. Lonsinger et al. improved upon the latter point and used a slightly larger cluster model (eight T-sites, whereas between one and five T-sites had been used previously). Lonsinger et al. concluded that several tetrahedral sites are energetically comparable (within 11 kcal/mol) to T12 for Al substitution, suggesting that Al siting in ZSM-5 is potentially controlled by kinetic rather than thermodynamic factors.[124] Although not stated as explicitly, this conclusion was also supported by Fripiat et al., who used the Hartree−Fock method to calculate that the range of energy change upon replacing Si with Al was within 12 kcal/mol among all 12 T-sites of ZSM-5.[80] This conclusion was also supported by another Hartree−Fock-based study that computed the energy to replace Si with Al at each of the 12 T-sites, identifying T6, T9, and T12 to be the most favorable and T3 the least favorable for substitution, although within only a 3.3 kcal/mol energy range.[125]

Another popular location for Al siting is the T7 site,[105,126] generally chosen for its stability.[26,98] Brändle and Sauer

DOI: 10.1021/acscatal.7b03676
ACS Catal. 2018, 8, 770−784

concluded that T7 was a stable location for Al substitution, from a comparison with T12.[98] Tranca et al. compared hexane adsorption at T7 and T12, finding only a weak energy difference (~2 kcal/mol) between the two sites.[105] Ghorbanpour et al. computed the stability of Al substitution at all 12 sites, finding T7 to be the most stable and T9 the least, although the span was less than 9 kcal/mol, suggesting that substitution at different T-sites is energetically similar.[26] These computational findings are consistent with the experimental observations that Al siting in ZSM-5 depends on the synthesis conditions used and not by the thermodynamic stability of different T-sites.[25,59,127,128] In addition to T12 and T7, some modeling studies have substituted Al at other T-sites,[87,90,109,119,129−136] albeit less commonly. A recent computational study[26] considered all 12 T-sites and used stability, accessibility, and acid strength as discerning criteria to conclude that T1 and T12 were the most favorable for Al substitution, while T2, T5, and T9 were also favorable.

Acid strength has also been mentioned as a criterion used in choosing T-sites. Jones and Iglesia performed periodic DFT calculations indicating that the deprotonation energy for every T-site for six different zeolites (including ZSM-5) differs by at most 3 kcal/mol.[44] At first glance, these acid strength estimates indicate that the choice of T-site may be unimportant, however, confinement effects imposed by local void structures can result in catalytic differences. This highlights the importance of utilizing dispersion corrections in DFT studies, depending on the research question under investigation. For example, in computing adsorption energies, long-range dispersion interactions require consideration for comprehensive treatment. Others have found it necessary to augment the DFT functional to include dispersion, as done by various research groups examining adsorption behavior in ZSM-5.[116,117,120] Long-range electrostatic interactions have also been shown to be important for stabilizing ions in theoretical treatments.[112] Continued efforts to use comprehensive structures when modeling ZSM-5 will enable building stronger connections between theory and the heterogeneous materials often studied by experiment and in turn achieving a more thorough understanding of Al siting in zeolites.

5. AL PROXIMITY WITHIN THE FRAMEWORK AND EFFECTS ON CATALYSIS

In addition to determining Al substitution within unique T-site locations of a given zeolite framework, studies have attempted to measure the local arrangements of framework Al atoms in proximal, or paired, configurations.[17,137] A widely used definition of framework Al "pairs" in ZSM-5 refers to framework Al with one or two Si neighbors that separate a second Al atom (Al-O-(Si-O)$_x$-Al, x = 1,2), while isolated Al have three or more intervening Si neighbors (Al-O-(Si-O)$_x$-Al, $x \geq 3$).[17] Al atoms that are not found in pairs can be "unpaired", which refer to Al atoms located in different rings but close enough to balance the charge of a divalent counterion, or "single" Al atoms (Figure 6).[127]

5.1. Catalysis. The effect of framework Al pairing on catalysis has been studied for a variety of reactions and zeolite frameworks. Paired Al sites in ZSM-5 have been reported to cause differences in the polarization of adsorbed alkanes for cracking and dehydration[138,139] and to influence the rate and selectivity for propene oligomerization.[140] Paired Al sites in CHA zeolites have also been reported to show a higher selectivity toward propene during the conversion of methanol-

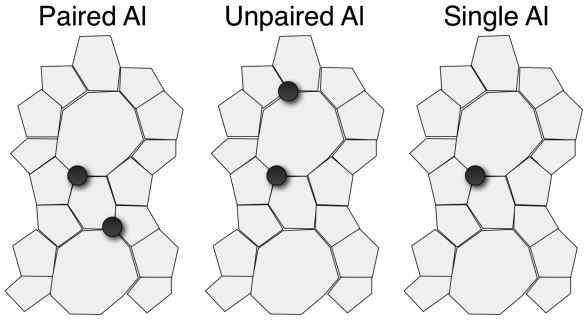

Figure 6. Classifications of different framework Al arrangements in ZSM-5 zeolites. Figure adapted with permission from Dědeček et al.[127] Copyright 2012 American Chemical Society.

to-olefins.[141,142] These examples suggest that Al proximity can influence catalytic behavior, although more precise models that decouple the effects of acid site pairing and location in zeolite frameworks can help clarify interpretations of data to rationalize the different catalytic behavior observed among different zeolite samples.

In the case of CHA zeolites, Di Iorio et al. reported that both first-order and zero-order rate constants (415 K) for methanol dehydration to dimethyl ether increased with increasing fractions of paired Al (Figure 7).[143] This rate

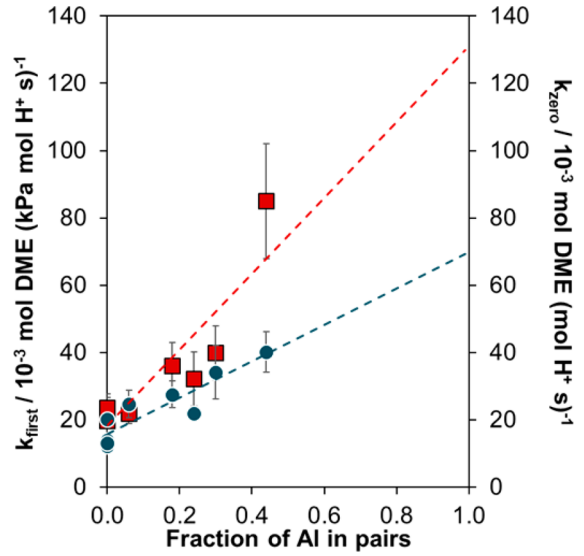

Figure 7. Rate constants for methanol dehydration systematically increase with increasing fraction of paired Al in CHA zeolites of constant Al content. Figure reproduced with permission from Di Iorio et al.[143] Copyright 2017 American Chemical Society.

constant enhancement was attributed to a shift in the dehydration mechanism from the associative pathway to the dissociative pathway. This mechanistic proposal was corroborated by in situ infrared (IR) spectra showing that the area of surface methoxy deformation modes, characteristic of the dissociative pathway, increased linearly with paired acid site content. First-order rate constants at isolated protons in small-pore CHA were higher than those measured previously for medium-pore and large-pore zeolites in the literature, while zero-order rate constants were similar to all other zeolites measured, demonstrating the utility in using a quantitative

DOI: 10.1021/acscatal.7b03676
ACS Catal. 2018, 8, 770−784

probe reaction to benchmark and interpret catalytic phenomena.[144]

5.2. Characterization. In quantifying Al sites in ZSM-5, titration techniques are frequently utilized to make inferences about surrogate extra-framework cationic species. Monovalent and divalent cationic species can be introduced by aqueous-phase ion-exchange, and molecular titrants can be introduced through vapor-phase adsorption. Monovalent cations (e.g., Cs^+, Na^+) introduced by liquid-phase ion-exchange procedures can estimate the number of acid sites and compare it to total framework Al content. Framework Al atoms may be an inaccurate measure of active Brønsted acid sites; therefore, direct titration of H^+ sites, during a catalytic reaction when possible, will provide more direct information about the active sites.[145]

In the MFI framework, three different divalent cation exchange sites (i.e., paired Al sites) have been identified, each characterized by their unique location within the framework and are referred to as α, β, and γ.[17] The α site is located along the "wall" of the 10-MR straight channel (the α ring is orthogonal to the direction of the straight channels) and comprises an elongated 6-MR with one bridging T-site. The β site also comprises a 6-MR, albeit without any bridging T-sites, and the normal vector from its opening is parallel to the direction of the straight channels. The γ site is boat-shaped, formed by a "hull" made of 8 T-sites and a "keel" of 4 T-sites.[17]

To quantitatively estimate the fraction of Al in different arrangements in ZSM-5, a method developed by Wichterlova and co-workers[146] proposes to titrate Al pairs by a Co^{2+} cation, while all other Al atoms remain compensated with protons (or another monovalent cation, such as Na^+). The diffuse reflectance UV−visible spectra of dehydrated Co-zeolites have been deconvoluted into peaks assigned to three possible Co^{2+} species for α, β, and γ sites (Figure 8).[24,127] These

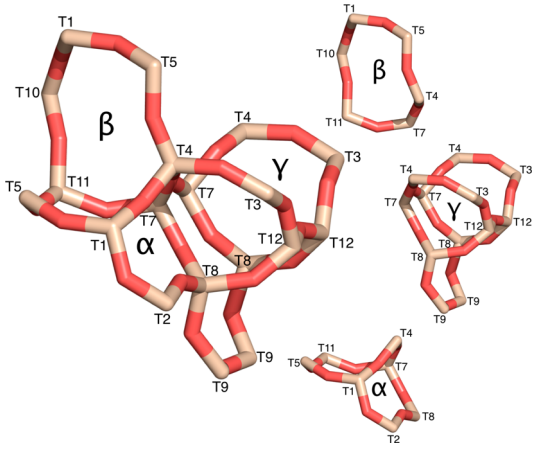

Figure 8. Mapping T-sites to α, β, and γ nomenclature. Computational studies of ZSM-5 tend to use the T-site nomenclature. Experiments have been mainly limited to determining the local environment of divalent extra-framework metal probes, which are classified as α, β, and γ sites (nomenclature as in Dědeček et al.[17]).

assignments are based on previous assignments made for the FER and MOR frameworks, because of the similarities in the framework ring structures to which Co^{2+} species bind.[146] A site balance can also be used to quantify the amount of Al in paired arrangements with the assistance of the liquid-phase ion exchange of Co^{2+}. Temperature-programmed desorption of NH_3 is used to quantify the number of H^+ sites on H-form and Co-zeolites via methods previously outlined for CHA and MFI frameworks.[147,148] These two separate NH_3 titration values can be compared to give an expected 2:1 exchange stoichiometry of H^+ sites for Co^{2+} in extra-framework positions and, when combined with UV−visible spectra showing evidence for bare Co^{2+} sites and the absence of cobalt oxides, provides a functional probe of the number of paired Al atoms present. Such quantitative titrations are techniques that can be widely adopted to benchmark results among different research groups, which will aid in developing a more unified understanding of Al distribution in different zeolite frameworks.

5.3. Synthesis. Methods to influence the Al proximity in ZSM-5 have been studied extensively by Dědeček and co-workers.[17] Early demonstrations provided evidence that the conditions of synthesis could influence the Al proximity in the crystalline product.[137] Further work was published describing the effects of changing the sources of the Na, Al, Si, and the organic SDA in the synthesis solution; at approximately the same Al molar content, ZSM-5 samples were crystallized with similar total Al content but varying amounts of Al pairs (Table 1).[128,149] This work also reported that adding varying amounts of Na^+ to the synthesis solution resulted in differences in paired Al content. These results, together with the authors' previous work, led to the conclusion that the Al siting during synthesis is not random, but not governed by any clear or predictive rules.[17]

Recent work by Di Iorio et al. on the single T-site CHA zeolite (SSZ-13) studied how using inorganic Na^+ cations and organic *N,N,N*-trimethyl-1-adamantylammonium ($TMAda^+$) cations in the synthesis medium influences Al proximity within crystalline zeolite products.[143,150] CHA zeolites crystallized in the presence of only $TMAda^+$ cations contained predominantly isolated framework Al atoms, evident in their inability to exchange divalent Co^{2+} cations and consistent with the size constraints that allow occupation of each CHA cage by only one $TMAda^+$ cation.[151] The replacement of $TMAda^+$ with Na^+ in the synthesis medium, at fixed total SDA cation and Al content, crystallized CHA zeolites with paired Al sites that increased systematically with the amount of Na^+ occluded within crystalline products. This observation was rationalized by proposing that Na^+ cations site framework Al centers in locations that are proximal to framework Al centers that charge-compensate positive charges in occluded $TMAda^+$ molecules, so as to preserve dispersive interactions between the hydrophobic adamantyl group of $TMAda^+$ and nonpolar portions of the siloxane framework. Thus, the cationic charge density of the occluded SDAs can be varied using mixtures of low-charge density (e.g., $TMAda^+$) and high-charge density (e.g., Na^+) cations, in order to influence the anionic charge density of the zeolite lattice that is defined by the local framework Al arrangement. This study of CHA zeolites avoids the structural complexities introduced by the presence of multiple framework T-sites, as is also the case for single T-site FAU zeolites,[152] providing a strategy to more directly probe the effects of synthesis conditions on Al proximity.

5.4. Modeling. Computational studies of ZSM-5 with lower Si/Al ratios, in which multiple framework Al atoms are considered in the model, are relatively scarce in the absence of extra-framework metals. Early work by Hass et al. included multiple Al atoms in the zeolite framework to assess their stability, concluding generally that Al−O−Al linkages are unstable relative to other configurations, consistent with

DOI: 10.1021/acscatal.7b03676
ACS Catal. 2018, 8, 770−784

Table 1. Siting of Framework Al Pairs in ZSM-5[a]

	Mixtures				Products					
	Al	Si	Na	Na/Al	Si/Al	Na/Al	Al_{2Al} (%)	α (%)	β (%)	γ (%)
A	$AlCl_3$	TEOS	-	0	21.2	-	42	28	69	3
B	$Al(NO_3)_3$	TEOS	-	0	28.6	-	6	-	-	-
C	Al metal	TEOS	-	0	34.3	-	56	48	51	1
D	$AlCl_3$	TEOS	-	0	29.3	-	46	25	69	6
E	$Al(OH)_3$	TEOS	-	0	54.0	-	24	48	51	1
F	$NaAlO_2$	TEOS	$NaAlO_2$	1	20.4	0.31	57	32	65	3
G	$AlCl_3$	Tixosil	-	0	23.9	-	71	48	52	0
H	$AlCl_3$	Na-Sil	Na-Sil	23	15.1	0.38	4	-	-	-
I	$AlCl_3$	TEOS	NaCl	9.9	22.8	0.53	18	10	81	9
J	$AlCl_3$	TEOS	Na_3PO_4	9.9	28.7	0.64	22	21	71	8
K	$AlCl_3$	TEOS	NaOH	9.9	20.9	2.78	58	24	70	6

[a]Synthesis conditions dictate where the framework Al atoms situate. Table reproduced with permission from Pashkova et al.[128]. Copyright 2015 Elsevier.

Lowenstein's rule.[83] In a similar vein, but more comprehensively, Ruiz-Salvador et al. utilized force field calculations to determine framework Al distributions in ZSM-5, attempting to mimic the conditions of synthesis at the stage when Al incorporation into the framework occurs by not including protons as charge compensating ions.[153] Upon comparing their computational results to Dempsey's rule, which states that framework Al atoms will tend to maximize their interatomic distance, deviations from Dempsey's rule appeared driven primarily by the anisotropy in the zeolite lattice.[153] The authors concluded that Al siting within the framework was determined by two primary (and sometimes competing) factors: the individual site thermodynamic preference (stability upon Si-to-Al substitution at a single site) and the Al−Al distance (Dempsey's rule).[153]

In one of the most exhaustive treatments on the topic to date, Fletcher et al. presented a periodic DFT investigation of all possible arrangements of two framework Al atoms per unit cell (Si/Al = 17) in H−CHA and Na-CHA,[154] including many "non-Lowensteinian" configurations containing Al−O−Al sequences. The lowest energy configurations included Al−O−Al sequences for H−CHA (but not for Na-CHA), an apparent violation of Lowenstein's rule. This finding was corroborated for four other zeolite frameworks (LTA, RHO, ABW, MOR) and also at lower Si/Al ratios (8, 11).[154] Given the well established maxim that framework Al distribution is synthesis-dependent[17,25,59,127,128] and thus driven to some extent by kinetic considerations, experiments corresponding to these theoretical calculations would be illuminating. Some of the unique Al arrangements identified to be energetically stable by Fletcher et al. may be able to catalyze alternate reaction pathways that are sensitive to two Brønsted acidic protons in close proximity.

The influence of framework Al distribution on catalysis by Brønsted acidic protons in ZSM-5 has rarely been addressed in the computational literature. The effects of Al proximity on catalysis was studied for alkane cracking by Song et al. by comparing free energy barriers at a single Al site (T12) and at paired Al sites separated by either two Si-occupied T-sites (second Al at T7) or three Si-occupied T-sites (second Al at T8).[139] In conjunction with ^{1}H DQ MAS NMR, UV−visible measurements of Co^{2+} exchanged zeolites, ^{13}C MAS NMR, and adsorption isotherm and calorimetry measurements, ONIOM calculations indicated that cracking rates at Al pairs were enhanced compared with rates at single sites, primarily due to more positive intrinsic activation entropies resulting from polarization of reactants and transition states by the adjacent acid site.[139] In addition, increasing the concentration of Al pairs was reported to enhanced the selectivity toward cracking over dehydrogenation, and furthermore toward central cracking over terminal cracking.[139]

Opalka et al. constructed models containing framework Al atoms located at an array of T6 and T12 locations at Si/Al ratios of 11 (two models), 23, and 95. Using periodic DFT, a detailed analysis was conducted on the effects of Al density and distribution on the adsorption and protonation of *i*-propylamine and *n*-pentane. For example, increasing the Al density resulted in increasing stabilization of the Brønsted acid site and weaker hydrogen bonding, suggesting an increase in Brønsted acid strength. Based on geometrical effects, T12 was predicted to be more reactive than T6, and reactivity was predicted to increase with increasing Al density. The pairing of T6 Brønsted acid sites in next−next nearest-neighbor positions (Si/Al = 11) produced what was predicted to be the most reactive site for adsorption and protonation of *n*-pentane.[119] Reaction barriers for hydrocarbon cracking were not computed, but the authors noted that these calculations are now underway.[119]

In comparison with the above, a number of computational studies of ZSM-5 with multiple framework Al atoms have included extra-framework metal species. Experimentally, extra-framework metals have been shown to enhance catalytic rates in zeolites,[12] though the chemical origins of these effects remain a topic of ongoing research. Extra-framework metals broaden the catalytic diversity of zeolites, as Li et al. note that exchanging Brønsted acid protons for extra-framework metals can facilitate a wider range of chemical reactions.[155] Rate enhancements due to extra-framework metals have been attributed to Lewis acid functionality,[132] but extra-framework metals have also been proposed to enhance the Brønsted acid strength of nearby protons[156] and enhance confinement and solvation effects due to partial occlusion of void space.[145]

The location and valence of the extra-framework metals influence catalysis and depend on the siting and distribution of the framework Al atoms that charge-compensate them. Sobalik et al. studied how synthesis affects the prevalence of framework Al pairs, the binding of monovalent and divalent cations, and their effects on catalytic reactivity in MFI,[157] as Sklenak et al. did in FER.[158] Joshi and Thompson reported an illustrative example of the connections between framework Al siting, extra-framework metal site binding, and overall reaction rate.

DOI: 10.1021/acscatal.7b03676
ACS Catal. 2018, 8, 770−784

To study alkane dehydrogenation mechanisms in Ga-ZSM-5, they placed a single Al at T12 when a monovalent cationic species was present, and two Al atoms at either T11-T11 or T12-T7 when divalent gallium monohydride was present.[159] For ethane dehydrogenation, the relative stability of the extra-framework gallium species was quantified by the heat of reaction for H_2 reduction, and it was reported to affect two steps of the reaction mechanism in an opposite manner (Figure 9). Higher stability leads to a high barrier for C−H

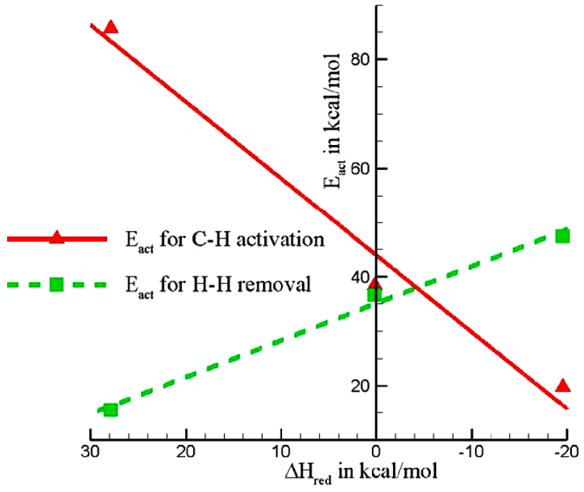

Figure 9. Overall reaction rate determined by Al siting, for ZSM-5 catalyzed conversion of ethane dehydrogenation with extra-framework Ga. Figure reproduced with permission from Joshi and Thomson.[159] Copyright 2005 Elsevier.

activation (first step) but a low barrier for H−H removal (final step), while intermediate stability results in an optimum exists for the barrier of the rate-determining step, exemplifying the Sabatier principle. Furthermore, the authors relate the activation barrier for C−H activation to the distance between framework Al atoms; among those studied with two framework Al atoms, the most stable is the 6-MR with framework Al atoms 4.53 Å apart, followed by 8-MR rings of with framework Al atoms 4.60 and 5.53 Å apart.

Li et al. connected the zeolite framework chemistry to the binding of extra-framework metals and reactivity. They analyzed the preferred locations for mononuclear and binuclear Fe complexes,[155,160] as well as their reactivity in the conversion of benzene to phenol.[155] Their initial work concurred with experiment that the 6-MR (α, β, δ) were the lowest energy sites for Fe^{2+} coordination, given the symmetric square-planar configuration these cations were able to adopt at these sites. These three sites were very similar in the catalytic enhancement for benzene conversion to phenol, while binuclear Fe species were shown to have higher barriers. Li et al. subsequently investigated conversion of methane to methanol in Cu/ZSM-5, placing extra-framework binuclear and trinuclear Cu species at the T7-T12 γ site, noting that this is the "preferred site for stabilization of a wide range of multinuclear transition metal-containing oxo complexes," as determined by their previous studies (Figure 10).[161]

Determining the active extra-framework metal species in a zeolite is difficult experimentally, and can benefit from contributions from theoretical studies. For example, Pidko et al. studied a variety of extra-framework metals in ZSM-5 to demonstrate that mononuclear oxygenated and hydroxylated

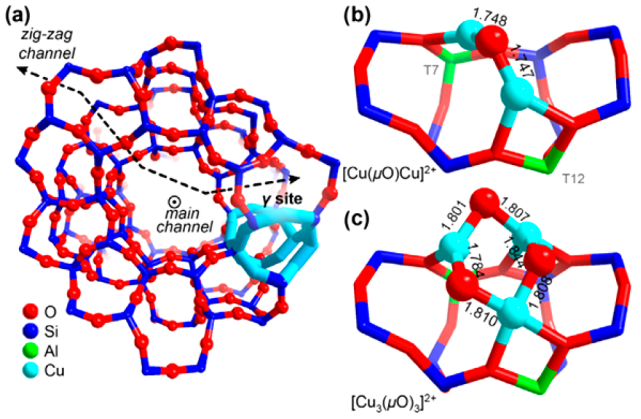

Figure 10. DFT study of extra-framework copper promoted conversion of methane to methanol in ZSM-5. Framework Al atoms were sited at T7 and T12 in the γ ring. Figure reproduced with permission from Li et al.[161] Copyright 2016 Elsevier.

cationic metal complexes tend to self-organize into binuclear complexes and that these complexes are much more reactive than their mononuclear counterparts.[162] In addition, Liu et al. studied mononuclear and multinuclear extra-framework Al species in high-aluminum FAU, connecting the thermodynamic cycles between various species with elementary reaction steps.[156] They concluded that trinuclear and tetranuclear Al species occupying the small sodalite cages are most favored, and then demonstrated that such species lower the reaction barrier for propane cracking via Brønsted acid protons.[156] These studies may guide experimental design toward reaction conditions that promote the presence of different extra-framework metal sites.

6. OUTLOOK

Recent research in zeolite catalysis has demonstrated that, even within a given framework, Al atoms sited in different crystallographic framework locations and at different relative proximities can generate catalytic active sites of different reactivity. The mechanistic origins of such phenomena can be better understood through: (i) the improved control of framework Al siting during synthesis, (ii) the development of robust methods to characterize Al location and proximity and their use to benchmark data collected in different research groups,[144] (iii) the development and use of catalytic probe reactions that precisely interrogate acid strength and confinement effects, and (iv) the development of theoretical treatments of extended structures, long-range electrostatic interactions, and weak dispersion forces. These research directions motivate the need for higher resolution and molecular-level detail in experiment, and more comprehensive treatment of material structures and catalytic chemistry by theory, in order to connect insights between experiment and theory to understand the consequences of Al location and proximity.

In the area of zeolite synthesis, a general observation in the literature is that the siting of Al atoms at specific T-sites or at varying relative proximity is not randomly determined, but dependent on the conditions of synthesis often in nuanced and poorly understood ways.[17] This motivates further research to continue understanding the mechanistic details of zeolite crystallization,[163,164] the extent to which kinetic and thermodynamic factors influence the structure of crystalline

DOI: 10.1021/acscatal.7b03676
ACS Catal. 2018, 8, 770−784

products, and what molecular interactions (e.g., those provided by structure-directing agents[76]) guide Al incorporation into lattice positions at various stages in the crystallization process. The use of in situ and in operando techniques to study crystal growth mechanisms are promising strategies to provide new mechanistic insights, as Lupulescu and Rimer have shown recently by using in situ atomic force microscopy to study the growth mechanisms of silicalite-1 (MFI).[165] In charge density mismatch theory, organic and inorganic cations of different charge-to-size ratio are used to crystallize new framework topologies and in wider elemental composition ranges;[166−170] adapting these concepts to also influence the siting[79,171] and arrangement[143,150] of Al atoms provides new avenues to study the role of SDAs on Al incorporation into lattice positions. Finally, understanding the roles of organic SDAs on Al siting in the framework can be aided by using experimental techniques such as solid-state NMR[152,172] or XRD[63] to provide structural information on organic molecules occluded within real zeolite products, and by making connections with information provided by theoretical approaches that model SDA interactions with idealized zeolite frameworks during and after synthesis.[173−175]

Additional research efforts in these areas can aid in the development of more predictive synthesis-structure relations. The development of such relations can be further facilitated by synthesis experiments in which only a single parameter is varied while other parameters are fixed, and by investigating higher symmetry single T-site zeolites (e.g., CHA) that avoid the added complexities of Al siting at crystallographically different T-site locations.[143,150] The synthesis-structure relations developed on structurally simpler frameworks may help form the basis of models to describe the behavior of more complex and lower-symmetry framework structures (e.g., MFI). Overall, such synthesis-structure relations can refine the empirical guidance derived from observations that Al siting is dependent on the conditions of synthesis, into more mechanism-based and predictive models.

In order to characterize different Al site locations and ensembles in zeolites, indirect probes of Al arrangements (e.g., Co^{2+} titrations of proximal Al sites), if performed quantitatively and corroborated by complementary characterization techniques, serve an important role in providing reproducible methods to benchmark findings among different research groups. Increased resolution into the active site structures probed using these indirect methods can be obtained by connecting experimental observations to theoretical predictions of binding energies of cations at various potential binding sites that exist within the heterogeneous distribution inherent to a real material (e.g., Cu^{2+} ions at different Al−Al pair arrangements in CHA[176]). Modeling such distributions are difficult for lower-symmetry structures (e.g., MFI), and can benefit first from simpler models developed and calibrated on higher-symmetry structures (e.g., CHA). Indirect probes of Al sites by spectroscopic methods (NMR, IR), especially in combination with probe molecules adsorbed at active sites,[177,178] can aid in the characterization of Al-site location and distribution. Direct probes of Al atoms can also help in developing more detailed synthesis-structure relations, as the increased sensitivity of ^{27}Al MAS NMR and the use of the DQ ^{27}Al MAS NMR techniques have provided more (yet, still incomplete) resolution into the assignments of Al incorporated at different T-sites in zeolites. Characterization of as-synthesized materials that can correlate internuclear distances between framework Al or O atoms and the atoms in occluded SDAs, similar to previous studies on FER zeolites,[63] will provide direct insight into SDA-framework interactions that can be incorporated into more robust synthesis-structure relations.

Understanding the catalytic consequences of Al siting and proximity requires robust probes of fundamental catalyst properties. Although there are many examples of the different reactivity among ZSM-5 zeolites of different Al arrangements, there are instances where research groups have arrived at different conclusions regarding the effects of Al location and proximity, even for the same set of materials studied using nominally the same characterization and catalytic probes. One example is the increase in alkane cracking and dehydrogenation rates with bulk Al content on ZSM-5 zeolites, which has been attributed to preferential Al siting into channel intersections[50] and to preferential formation of Al pairs.[139] The benchmarking of kinetic data[144] and the use of quantitative kinetic probes (e.g., methanol dehydration), rather than inferential probe reactions that rely on shape selective properties (e.g., constraint index tests), will provide sharper resolution into the different catalytic properties of different Al site ensembles. In order to properly interpret these kinetic probes, mechanism-derived expressions to model rate data measured in the absence of transport artifacts, and accurate quantification of purported active sites, are required.[43]

The usefulness of computational catalysis is largely due to its specificity and ability to probe atomic detail at length and time scales that are generally inaccessible to experiment. These significant advantages, however, can only be leveraged to the extent that the modeled atomic details are consistent with relevant and corresponding experimental conditions; exquisite theoretical treatments of irrelevant reaction conditions are of little value to develop realistic models of catalytic phenomena. The most useful theory-based studies will construct structural models that are relatable to experimental characterizations. There is a need for more comprehensive studies wherein a given property (or set of properties) are characterized across a wide swath of possible atomic configurations, such as the siting of framework Al atoms at particular T-sites and various distributions of them. Studies of this ilk[26,44] are extremely useful and help focus theoretical studies on problems that contribute to moving the field forward and addressing bottlenecks in connecting theory to experiment, rather than being motivated by tractability but with only marginal connections to experiment. For example, such comprehensive studies could be especially helpful to examine the stabilization of transition states as a function of framework Al configuration and confinement within zeolite pores.[57]

The challenges in modeling become even more complicated when extra-framework metals are included. Theoretical studies of zeolites increasingly include extra-framework metals due to their relevance for various reaction classes.[12] Reaction mechanisms at different catalytic sites (e.g., Lewis, Brønsted, bifunctional[179]) and their effects on turnover rates depend on the location of these sites, which is in turn influenced by the Al distribution in the zeolite framework. Thoughtful consideration of where to site the framework Al and extra-framework metal are inextricably linked, and influence the conclusions of a theoretical study. Model design in this context must consider the active extra-framework metal species (e.g., valence, structure) and the location of this active species within the zeolite *during the catalytic reaction*. Computational studies often

DOI: 10.1021/acscatal.7b03676
ACS Catal. 2018, 8, 770−784

begin by looking for the most stable reactant configuration, such as the lowest energy state for a given T-site substitution of Al or most stable configuration for adsorption of substrate. The catalytically relevant configurations, however, will be those that preferentially stabilize the *transition state* of a given reaction, not the reactant state, all other factors equivalent. This point is underscored by efforts that use SDAs that mimic the transition state, to prepare zeolites whose pores may optimally stabilize the transition state.[173] The functional form of rate equations reminds us that although rates depend on pre-exponential factors (which would include T-site stability and occupation by Al), they are more sensitive to activation barriers. As an example, consider the conclusion by Pashkova et al. that Al pairs are 100-fold less likely to be located at γ sites than at α/β sites in MFI (at Si/Al = 54).[128] If all other factors are equivalent, this less populated γ site will contribute equally to measured reaction rates (at 573 K) if the activation barrier at this site is just 5 kcal/mol less than the barrier at the 100-fold more populated α/β sites. Considerations such as these, framed from catalytic perspectives, will allow researchers to construct models that address the salient features of experimental measurements.

In summary, this outlook frames the challenges and opportunities in zeolite research to develop more predictive synthesis-structure-function relations, to identify the origins of catalytic diversity arising from different framework Al arrangements and distributions in zeolites, and to connect the findings on real samples studied by experiment to the ideal model structures studied by theory. We expect that this Perspective will continue to stimulate experimental and theoretical research that forges stronger connections between zeolite structure, composition, and active sites to catalytic function. By doing so, such research will help transform the field of zeolite active-site design from an empirical endeavor into a more predictable science founded on validated models.

AUTHOR INFORMATION

Corresponding Authors

*E-mail: seonah.kim@nrel.gov.

*E-mail: rgounder@purdue.edu.

ORCID

Mark R. Nimlos: 0000-0001-7117-775X

Seonah Kim: 0000-0001-9846-7140

Rajamani Gounder: 0000-0003-1347-534X

Author Contributions

¶(B.C.K., C.T.N.) These authors contributed equally.

Notes

The authors declare no competing financial interest.

ACKNOWLEDGMENTS

RG and CN acknowledge financial support from the National Science Foundation under award number 1552517-CBET. BK, DR, MN, and SK acknowledge financial support from the Computational Physics and Chemistry (CCPC) supported by the U.S. Department of Energy's Bioenergy Technologies office (DOE BETO), contract number DE-AC36-08G028308. We thank John Di Iorio for helpful technical discussions and reviewing of the manuscript.

REFERENCES

(1) Corma, A. *Chem. Rev.* **1995**, *95*, 559−614.

(2) Degnan, T. F. *J. Catal.* **2003**, *216*, 32−46.

(3) Dwyer, F. G.; Degnan, T. F. Shape Selectivity in Catalytic Cracking. In *Fluid Catalytic Cracking: Science and Technology*; Magee, J. S., Mitchell, M. M., Jr., Eds.; Elsevier: Amsterdam, 1993; Vol. *76*.

(4) Garwood, W. E. Conversion of C_2-C_{10} to Higher Olefins Over Synthetic Zeolite ZSM-5. *Intrazeolite Chemistry*; ACS Publications: Washington, DC, 1983; pp 383−396.

(5) Tabak, S. A.; Krambeck, F. J.; Garwood, W. E. *AIChE J.* **1986**, *32*, 1526−1531.

(6) Chang, C. D. *Catal. Rev.: Sci. Eng.* **1983**, *25*, 1−118.

(7) Huber, G. W.; Corma, A. *Angew. Chem., Int. Ed.* **2007**, *46*, 7184−7201.

(8) Taarning, E.; Osmundsen, C. M.; Yang, X.; Voss, B.; Andersen, S. I.; Christensen, C. H. *Energy Environ. Sci.* **2011**, *4*, 793−804.

(9) Bruijnincx, P. C. A.; Weckhuysen, B. M. *Angew. Chem., Int. Ed.* **2013**, *52*, 11980−11987.

(10) Woertink, J. S.; Smeets, P. J.; Groothaert, M. H.; Vance, M. A.; Sels, B. F.; Schoonheydt, R. A.; Solomon, E. I. *Proc. Natl. Acad. Sci. U. S. A.* **2009**, *106*, 18908−18913.

(11) Sato, S.; Yu-u, Y.; Yahiro, H.; Mizuno, N.; Iwamoto, M. *Appl. Catal.* **1991**, *70*, L1−L5.

(12) Farberow, C. A.; Cheah, S.; Kim, S.; Miller, J. T.; Gallagher, J. R.; Hensley, J. E.; Schaidle, J. A.; Ruddy, D. A. *ACS Catal.* **2017**, *7*, 3662−3667.

(13) Perez-Ramirez, J.; Christensen, C. H.; Egeblad, K.; Christensen, C. H.; Groen, J. C. *Chem. Soc. Rev.* **2008**, *37*, 2530−2542.

(14) Martínez, C.; Corma, A. *Coord. Chem. Rev.* **2011**, *255*, 1558−1580.

(15) Na, K.; Choi, M.; Ryoo, R. *Microporous Mesoporous Mater.* **2013**, *166*, 3−19.

(16) Roth, W. J.; Nachtigall, P.; Morris, R. E.; Čejka, J. *Chem. Rev.* **2014**, *114*, 4807−4837.

(17) Dědeček, J.; Sobalik, Z.; Wichterlová, B. *Catal. Rev.: Sci. Eng.* **2012**, *54*, 135−223.

(18) Fyfe, C. A.; Feng, Y.; Grondey, H.; Kokotailo, G. T.; Gies, H. *Chem. Rev.* **1991**, *91*, 1525−1543.

(19) Fyfe, C. A.; Gobbi, G. C.; Klinowski, J.; Thomas, J. M.; Ramdas, S. *Nature* **1982**, *296*, 530−533.

(20) Kokotailo, G. T.; Lawton, S. L.; Olson, D. H.; Meier, W. M. *Nature* **1978**, *272*, 437−438.

(21) Davis, M. E. *Acc. Chem. Res.* **1993**, *26*, 111−115.

(22) First, E. L.; Gounaris, C. E.; Wei, J.; Floudas, C. A. *Phys. Chem. Chem. Phys.* **2011**, *13*, 17339−17358.

(23) Van Koningsveld, H.; Jansen, J. C.; Van Bekkum, H. *Zeolites* **1990**, *10*, 235−242.

(24) Pashkova, V.; Sklenak, S.; Klein, P.; Urbanova, M.; Dědeček, J. *Chem. - Eur. J.* **2016**, *22*, 3937−3941.

(25) Sklenak, S.; Dědeček, J.; Li, C.; Wichterlova, B.; Gabova, V.; Sierka, M.; Sauer, J. *Phys. Chem. Chem. Phys.* **2009**, *11*, 1237−1247.

(26) Ghorbanpour, A.; Rimer, J. D.; Grabow, L. C. *Catal. Commun.* **2014**, *52*, 98−102.

(27) Argauer, R. J.; Landolt, G. R. Crystalline Zeolite ZSM-5 and Method of Preparing the Same. U.S. Patent 3,702,886, 1972.

(28) Kerr, G. T. Process for Synthesizing a Methylammonium Crystalline Zeolite. U.S. Patent 3,228,969, 1966.

(29) Chen, N. Y. *Ind. Eng. Chem. Res.* **2001**, *40*, 4157−4161.

(30) Chen, N. Y.; Garwood, W. E. *J. Catal.* **1978**, *52*, 453−458.

(31) Bhatia, S. *Zeolite Catalysis: Principles and Applications*; CRC Press: Boca Raton, FL, 1990.

(32) Kaeding, W. W.; Chu, C.; Young, L. B.; Weinstein, B.; Butter, S. A. *J. Catal.* **1981**, *67*, 159−174.

(33) Tsai, T.-C.; Liu, S.-B.; Wang, I. *Appl. Catal., A* **1999**, *181*, 355−398.

(34) Chen, N. Y.; Degnan, T. F.; Koenig, L. R. *Chem. Technol.* **1986**, *16*, 506−511.

(35) Adjaye, J. D.; Bakhshi, N. N. *Fuel Process. Technol.* **1995**, *45*, 161−183.

(36) Adjaye, J. D.; Bakhshi, N. N. *Fuel Process. Technol.* **1995**, *45*, 185−202.

DOI: 10.1021/acscatal.7b03676
ACS Catal. 2018, 8, 770−784

(37) Gayubo, A. G.; Aguayo, A. T.; Atutxa, A.; Aguado, R.; Bilbao, J. *Ind. Eng. Chem. Res.* **2004**, *43*, 2610−2618.
(38) Gayubo, A. G.; Aguayo, A. T.; Atutxa, A.; Aguado, R.; Olazar, M.; Bilbao, J. *Ind. Eng. Chem. Res.* **2004**, *43*, 2619−2626.
(39) Jae, J.; Tompsett, G. A.; Foster, A. J.; Hammond, K. D.; Auerbach, S. M.; Lobo, R. F.; Huber, G. W. *J. Catal.* **2011**, *279*, 257−268.
(40) Haag, W. O.; Lago, R. M.; Weisz, P. B. *Nature* **1984**, *309*, 589−591.
(41) Weisz, P. B.; Miale, J. N. *J. Catal.* **1965**, *4*, 527−529.
(42) Olson, D. H.; Haag, W. O.; Lago, R. M. *J. Catal.* **1980**, *61*, 390−396.
(43) Boudart, M. *Chem. Rev.* **1995**, *95*, 661−666.
(44) Jones, A. J.; Iglesia, E. *ACS Catal.* **2015**, *5*, 5741−5755.
(45) Derouane, E. G. *J. Catal.* **1986**, *100*, 541−544.
(46) Gounder, R.; Iglesia, E. *Chem. Commun.* **2013**, *49*, 3491−3509.
(47) Zones, S. I.; Harris, T. V. *Microporous Mesoporous Mater.* **2000**, *35*, 31−46.
(48) Yokoi, T.; Mochizuki, H.; Biligetu, T.; Wang, Y.; Tatsumi, T. *Chem. Lett.* **2017**, *46*, 798−800.
(49) Yokoi, T.; Mochizuki, H.; Namba, S.; Kondo, J. N.; Tatsumi, T. *J. Phys. Chem. C* **2015**, *119*, 15303−15315.
(50) Janda, A.; Bell, A. T. *J. Am. Chem. Soc.* **2013**, *135*, 19193−19207.
(51) Liang, T.; Chen, J.; Qin, Z.; Li, J.; Wang, P.; Wang, S.; Wang, G.; Dong, M.; Fan, W.; Wang, J. *ACS Catal.* **2016**, *6*, 7311−7325.
(52) Chen, J.; Liang, T.; Li, J.; Wang, S.; Qin, Z.; Wang, P.; Huang, L.; Fan, W.; Wang, J. *ACS Catal.* **2016**, *6*, 2299−2313.
(53) Wang, S.; Wei, Z.; Chen, Y.; Qin, Z.; Ma, H.; Dong, M.; Fan, W.; Wang, J. *ACS Catal.* **2015**, *5*, 1131−1144.
(54) Carr, R. T.; Neurock, M.; Iglesia, E. *J. Catal.* **2011**, *278*, 78−93.
(55) Jones, A. J.; Carr, R. T.; Zones, S. I.; Iglesia, E. *J. Catal.* **2014**, *312*, 58−68.
(56) Jones, A. J.; Iglesia, E. *Angew. Chem., Int. Ed.* **2014**, *53*, 12177−12181.
(57) Jones, A. J.; Zones, S. I.; Iglesia, E. *J. Phys. Chem. C* **2014**, *118*, 17787−17800.
(58) Sierka, M.; Eichler, U.; Datka, J.; Sauer, J. *J. Phys. Chem. B* **1998**, *102*, 6397−6404.
(59) Sklenak, S.; Dědeček, J.; Li, C.; Wichterlová, B.; Gábová, V.; Sierka, M.; Sauer, J. *Angew. Chem., Int. Ed.* **2007**, *46*, 7286−7289.
(60) Dědeček, J.; Lucero, M. J.; Li, C.; Gao, F.; Klein, P.; Urbanova, M.; Tvaruzkova, Z.; Sazama, P.; Sklenak, S. *J. Phys. Chem. C* **2011**, *115*, 11056−11064.
(61) Biligetu, T.; Wang, Y.; Nishitoba, T.; Otomo, R.; Park, S.; Mochizuki, H.; Kondo, J. N.; Tatsumi, T.; Yokoi, T. *J. Catal.* **2017**, *353*, 1−10.
(62) Vjunov, A.; Fulton, J. L.; Huthwelker, T.; Pin, S.; Mei, D.; Schenter, G. K.; Govind, N.; Camaioni, D. M.; Hu, J. Z.; Lercher, J. A. *J. Am. Chem. Soc.* **2014**, *136*, 8296−8306.
(63) Pinar, A. B.; Gómez-Hortigüela, L.; McCusker, L. B.; Pérez-Pariente, J. *Chem. Mater.* **2013**, *25*, 3654−3661.
(64) Han, O. H.; Kim, C. S.; Hong, S. B. *Angew. Chem., Int. Ed.* **2002**, *41*, 469−472.
(65) Heo, N. H.; Kim, C. W.; Kwon, H. J.; Kim, G. H.; Kim, S. H.; Hong, S. B.; Seff, K. *J. Phys. Chem. C* **2009**, *113*, 19937−19956.
(66) Kim, C. W.; Heo, N. H.; Seff, K. *J. Phys. Chem. C* **2011**, *115*, 24823−24838.
(67) Lin, J.-C.; Chao, K.-J.; Wang, Y. *Zeolites* **1991**, *11*, 376−379.
(68) Mentzen, B. F.; Bergeret, G. *J. Phys. Chem. C* **2007**, *111*, 12512−12516.
(69) Mentzen, B. F.; Bergeret, G.; Emerich, H.; Weber, H.-P. *J. Phys. Chem. B* **2006**, *110*, 13741−13752.
(70) Mentzen, B. F.; Bergeret, G.; Emerich, H.; Weber, H.-P. *J. Phys. Chem. B* **2006**, *110*, 97−106.
(71) Olson, D. H.; Khosrovani, N.; Peters, A. W.; Toby, B. H. *J. Phys. Chem. B* **2000**, *104*, 4844−4848.
(72) Van Bokhoven, J. A.; Lee, T.-L.; Drakopoulos, M.; Lamberti, C.; Thieß, S.; Zegenhagen, J. *Nat. Mater.* **2008**, *7*, 551−555.
(73) Bohinc, R.; Hoszowska, J.; Dousse, J. C.; Błachucki, W.; Zeeshan, F.; Kayser, Y.; Nachtegaal, M.; Pinar, A. B.; van Bokhoven, J. A. *Phys. Chem. Chem. Phys.* **2017**, *19*, 29271−29277.
(74) Perea, D. E.; Arslan, I.; Liu, J.; Ristanović, Z.; Kovarik, L.; Arey, B. W.; Lercher, J. A.; Bare, S. R.; Weckhuysen, B. M. *Nat. Commun.* **2015**, *6*, Article No. 7589.
(75) Zhu, Q.; Kondo, J. N.; Yokoi, T.; Setoyama, T.; Yamaguchi, M.; Takewaki, T.; Domen, K.; Tatsumi, T. *Phys. Chem. Chem. Phys.* **2011**, *13*, 14598−14605.
(76) Burton, A. W.; Zones, S. I. *Stud. Surf. Sci. Catal.* **2007**, *168*, 137−179.
(77) Shantz, D. F.; Fild, C.; Koller, H.; Lobo, R. F. *J. Phys. Chem. B* **1999**, *103*, 10858−10865.
(78) Román-Leshkov, Y.; Moliner, M.; Davis, M. E. *J. Phys. Chem. C* **2011**, *115*, 1096−1102.
(79) Pinar, A. B.; García, R.; Gómez-Hortigüela, L.; Pérez-Pariente, J. *Top. Catal.* **2010**, *53*, 1297−1303.
(80) Fripiat, J. G.; Berger-André, F.; André, J.-M.; Derouanc, E. G. *Zeolites* **1983**, *3*, 306−310.
(81) Derouane, E. G.; Fripiat, J. G. *Zeolites* **1985**, *5*, 165−172.
(82) Vetrivel, R.; Pal, S.; Krishnan, S. *J. Mol. Catal.* **1991**, *66*, 385−397.
(83) Hass, E. C.; Mezey, P. G.; Plath, P. J. *J. Mol. Struct.: THEOCHEM* **1981**, *76*, 389−399.
(84) Hass, E. C.; Mezey, P. G.; Plath, P. J. *J. Mol. Struct.: THEOCHEM* **1982**, *87*, 261−272.
(85) Mortier, W. J.; Sauer, J.; Lercher, J. A.; Noller, H. *J. Phys. Chem.* **1984**, *88*, 905−912.
(86) O'Malley, P. J.; Dwyer, J. *J. Phys. Chem.* **1988**, *92*, 3005−3007.
(87) Vetrivel, R.; Catlow, C. R. A.; Colbourn, E. A. *Proc. R. Soc. London, Ser. A* **1988**, *417*, 81−94.
(88) Sauer, J.; Bleiber, A. *Catal. Today* **1988**, *3*, 485−492.
(89) Geschke, D.; Hoffmann, W. D.; Deininger, D. *Surf. Sci.* **1976**, *57*, 559−570.
(90) Vetrivel, R.; Catlow, C. R. A.; Colbourn, E. A. *J. Phys. Chem.* **1989**, *93*, 4594−4598.
(91) Gale, J. D.; Catlow, C. R. A.; Cheetham, A. K. *J. Chem. Soc., Chem. Commun.* **1991**, 178−179.
(92) Reischman, P. T.; Schmitt, K. D.; Olson, D. H. *J. Phys. Chem.* **1988**, *92*, 5165−5169.
(93) Geerlings, P.; Tariel, N.; Botrel, A.; Lissillour, R.; Mortier, W. J. *J. Phys. Chem.* **1984**, *88*, 5752−5758.
(94) Kustov, L. M.; Kazanskii, V. B.; Beran, S.; Kubelkova, L.; Jiru, P. *J. Phys. Chem.* **1987**, *91*, 5247−5251.
(95) Beran, S. *J. Mol. Catal.* **1985**, *30*, 95−99.
(96) Beran, S.; Kubelkova, L. *J. Mol. Catal.* **1987**, *39*, 13−19.
(97) Kazansky, V. B.; Senchenya, I. N. *J. Catal.* **1989**, *119*, 108−120.
(98) Brändle, M.; Sauer, J. *J. Am. Chem. Soc.* **1998**, *120*, 1556−1570.
(99) Charoenwiangnuea, P.; Maihom, T.; Kongpracha, P.; Sirijaraensre, J.; Limtrakul, J. *RSC Adv.* **2016**, *6*, 105888−105894.
(100) Joshi, K. L.; Psofogiannakis, G.; Van Duin, A. C. T.; Raman, S. *Phys. Chem. Chem. Phys.* **2014**, *16*, 18433−18441.
(101) Kim, S.; Evans, T. J.; Mukarakate, C.; Bu, L.; Beckham, G. T.; Nimlos, M. R.; Paton, R. S.; Robichaud, D. J. *ACS Sustainable Chem. Eng.* **2016**, *4*, 2615−2623.
(102) Kim, S.; Robichaud, D. J.; Beckham, G. T.; Paton, R. S.; Nimlos, M. R. *J. Phys. Chem. A* **2015**, *119*, 3604−3614.
(103) Li, Y.; Zhang, C.; Li, C.; Liu, Z.; Ge, W. *Chem. Eng. J.* **2017**, *320*, 458−467.
(104) Maihom, T.; Probst, M.; Limtrakul, J. *J. Phys. Chem. C* **2014**, *118*, 18564−18572.
(105) Tranca, D. C.; Zimmerman, P. M.; Gomes, J.; Lambrecht, D.; Keil, F. J.; Head-Gordon, M.; Bell, A. T. *J. Phys. Chem. C* **2015**, *119*, 28836−28853.
(106) Yang, Z.; Yang, G.; Liu, X.; Han, X. *Catal. Lett.* **2013**, *143*, 260−266.
(107) Zimmerman, P. M.; Tranca, D. C.; Gomes, J.; Lambrecht, D. S.; Head-Gordon, M.; Bell, A. T. *J. Am. Chem. Soc.* **2012**, *134*, 19468−19476.

DOI: 10.1021/acscatal.7b03676
ACS Catal. 2018, 8, 770−784

(108) Alexopoulos, K.; John, M.; Van der Borght, K.; Galvita, V.; Reyniers, M.-F.; Marin, G. B. *J. Catal.* **2016**, *339*, 173−185.
(109) Brand, H. V.; Curtiss, L. A.; Iton, L. E. *J. Phys. Chem.* **1992**, *96*, 7725−7732.
(110) Clark, L. A.; Sierka, M.; Sauer, J. *J. Am. Chem. Soc.* **2004**, *126*, 936−947.
(111) Cnudde, P.; De Wispelaere, K.; Van der Mynsbrugge, J.; Waroquier, M.; Van Speybroeck, V. *J. Catal.* **2017**, *345*, 53−69.
(112) Ferguson, G. A.; Cheng, L.; Bu, L.; Kim, S.; Robichaud, D. J.; Nimlos, M. R.; Curtiss, L. A.; Beckham, G. T. *J. Phys. Chem. A* **2015**, *119*, 11397−11405.
(113) Gonzales, N. O.; Bell, A. T.; Chakraborty, A. K. *J. Phys. Chem. B* **1997**, *101*, 10058−10064.
(114) John, M.; Alexopoulos, K.; Reyniers, M.-F.; Marin, G. B. *J. Catal.* **2015**, *330*, 28−45.
(115) Nguyen, C. M.; De Moor, B. A.; Reyniers, M.-F. o.; Marin, G. B. *J. Phys. Chem. C* **2012**, *116*, 18236−18249.
(116) Nguyen, C. M.; Reyniers, M.-F.; Marin, G. B. *Phys. Chem. Chem. Phys.* **2010**, *12*, 9481−9493.
(117) Nguyen, C. M.; Reyniers, M.-F.; Marin, G. B. *J. Phys. Chem. C* **2011**, *115*, 8658−8669.
(118) Nguyen, C. M.; Reyniers, M.-F.; Marin, G. B. *J. Catal.* **2015**, *322*, 91−103.
(119) Opalka, S. M.; Zhu, T. *Microporous Mesoporous Mater.* **2016**, *222*, 256−270.
(120) Svelle, S.; Tuma, C.; Rozanska, X.; Kerber, T.; Sauer, J. *J. Am. Chem. Soc.* **2009**, *131*, 816−825.
(121) Wang, C.; Chu, Y.; Zheng, A.; Xu, J.; Wang, Q.; Gao, P.; Qi, G.; Gong, Y.; Deng, F. *Chem. - Eur. J.* **2014**, *20*, 12432−12443.
(122) Wang, C.-M.; Wang, Y.-D.; Du, Y.-J.; Yang, G.; Xie, Z.-K. *Catal. Sci. Technol.* **2016**, *6*, 3279−3288.
(123) Zhang, W.; Chu, Y.; Wei, Y.; Yi, X.; Xu, S.; Huang, J.; Zhang, M.; Zheng, A.; Deng, F.; Liu, Z. *Microporous Mesoporous Mater.* **2016**, *231*, 216−229.
(124) Lonsinger, S. R.; Chakraborty, A. K.; Theodorou, D. N.; Bell, A. T. *Catal. Lett.* **1991**, *11*, 209−217.
(125) Alvarado-Swaisgood, A. E.; Barr, M. K.; Hay, P. J.; Redondo, A. *J. Phys. Chem.* **1991**, *95*, 10031−10036.
(126) Haase, F.; Sauer, J. *Microporous Mesoporous Mater.* **2000**, *35*, 379−385.
(127) Dědeček, J.; Balgová, V.; Pashkova, V.; Klein, P.; Wichterlová, B. *Chem. Mater.* **2012**, *24*, 3231−3239.
(128) Pashkova, V.; Klein, P.; Dědeček, J.; Tokarová, V.; Wichterlová, B. *Microporous Mesoporous Mater.* **2015**, *202*, 138−146.
(129) Brogaard, R. Y.; Weckhuysen, B. M.; Nørskov, J. K. *J. Catal.* **2013**, *300*, 235−241.
(130) Gao, J.; Zheng, Y.; Tang, Y.; Jehng, J.-M.; Grybos, R.; Handzlik, J.; Wachs, I. E.; Podkolzin, S. G. *ACS Catal.* **2015**, *5*, 3078−3092.
(131) Ghorbanpour, A.; Rimer, J. D.; Grabow, L. C. *ACS Catal.* **2016**, *6*, 2287−2298.
(132) Mahyuddin, M. H.; Staykov, A.; Shiota, Y.; Yoshizawa, K. *ACS Catal.* **2016**, *6*, 8321−8331.
(133) Mei, D.; Lercher, J. A. *AIChE J.* **2017**, *63*, 172−184.
(134) Sillar, K.; Burk, P. *J. Mol. Struct.: THEOCHEM* **2002**, *589*, 281−290.
(135) Yumura, T.; Hirose, Y.; Wakasugi, T.; Kuroda, Y.; Kobayashi, H. *ACS Catal.* **2016**, *6*, 2487−2495.
(136) Yumura, T.; Takeuchi, M.; Kobayashi, H.; Kuroda, Y. *Inorg. Chem.* **2009**, *48*, 508−517.
(137) Gábová, V.; Dědeček, J.; Čejka, J. *Chem. Commun.* **2003**, 1196−1197.
(138) Sazama, P.; Dědeček, J.; Gábová, V.; Wichterlová, B.; Spoto, G.; Bordiga, S. *J. Catal.* **2008**, *254*, 180−189.
(139) Song, C.; Chu, Y.; Wang, M.; Shi, H.; Zhao, L.; Guo, X.; Yang, W.; Shen, J.; Xue, N.; Peng, L.; Ding, W. *J. Catal.* **2017**, *349*, 163−174.
(140) Mlinar, A. N.; Zimmerman, P. M.; Celik, F. E.; Head-Gordon, M.; Bell, A. T. *J. Catal.* **2012**, *288*, 65−73.
(141) Deimund, M. A.; Harrison, L.; Lunn, J. D.; Liu, Y.; Malek, A.; Shayib, R.; Davis, M. E. *ACS Catal.* **2016**, *6*, 542−550.
(142) Dusselier, M.; Deimund, M. A.; Schmidt, J. E.; Davis, M. E. *ACS Catal.* **2015**, *5*, 6078−6085.
(143) Di Iorio, J. R.; Nimlos, C. T.; Gounder, R. *ACS Catal.* **2017**, *7*, 6663−6674.
(144) Bligaard, T.; Bullock, R. M.; Campbell, C. T.; Chen, J. G.; Gates, B. C.; Gorte, R. J.; Jones, C. W.; Jones, W. D.; Kitchin, J. R.; Scott, S. L. *ACS Catal.* **2016**, *6*, 2590−2602.
(145) Gounder, R.; Jones, A. J.; Carr, R. T.; Iglesia, E. *J. Catal.* **2012**, *286*, 214−223.
(146) Dědeček, J.; Kaucky, D.; Wichterlova, B. *Microporous Mesoporous Mater.* **2000**, *35*, 483−494.
(147) Bates, S. A.; Delgass, W. N.; Ribeiro, F. H.; Miller, J. T.; Gounder, R. *J. Catal.* **2014**, *312*, 26−36.
(148) Di Iorio, J. R.; Bates, S. A.; Verma, A. A.; Delgass, W. N.; Ribeiro, F. H.; Miller, J. T.; Gounder, R. *Top. Catal.* **2015**, *58*, 424−434.
(149) Pinar, A. B.; Márquez-Álvarez, C.; Grande-Casas, M.; Pérez-Pariente, J. *J. Catal.* **2009**, *263*, 258−265.
(150) Di Iorio, J. R.; Gounder, R. *Chem. Mater.* **2016**, *28*, 2236−2247.
(151) Zones, S. I. *J. Chem. Soc., Faraday Trans.* **1991**, *87*, 3709−3716.
(152) Oleksiak, M. D.; Muraoka, K.; Hsieh, M.-F.; Conato, M. T.; Shimojima, A.; Okubo, T.; Chaikittisilp, W.; Rimer, J. D. *Angew. Chem.* **2017**, *129*, 13551−13556.
(153) Ruiz-Salvador, A. R.; Grau-Crespo, R.; Gray, A. E.; Lewis, D. W. *J. Solid State Chem.* **2013**, *198*, 330−336.
(154) Fletcher, R. E.; Ling, S.; Slater, B. *Chem. Sci.* **2017**, *8*, 7483.
(155) Li, G.; Pidko, E. A.; van Santen, R. A.; Feng, Z.; Li, C.; Hensen, E. J. M. *J. Catal.* **2011**, *284*, 194−206.
(156) Liu, C.; Li, G.; Hensen, E. J. M.; Pidko, E. A. *ACS Catal.* **2015**, *5*, 7024−7033.
(157) Sobalik, Z.; Sazama, P.; Dědeček, J.; Wichterlová, B. *Appl. Catal., A* **2014**, *474*, 178−185.
(158) Sklenak, S.; Andrikopoulos, P. C.; Whittleton, S. R.; Jirglova, H.; Sazama, P.; Benco, L.; Bucko, T.; Hafner, J.; Sobalik, Z. *J. Phys. Chem. C* **2013**, *117*, 3958−3968.
(159) Joshi, Y. V.; Thomson, K. T. *Catal. Today* **2005**, *105*, 106−121.
(160) Li, G.; Pidko, E. A.; van Santen, R. A.; Li, C.; Hensen, E. J. M. *J. Phys. Chem. C* **2013**, *117*, 413−426.
(161) Li, G.; Vassilev, P.; Sanchez-Sanchez, M.; Lercher, J. A.; Hensen, E. J. M.; Pidko, E. A. *J. Catal.* **2016**, *338*, 305−312.
(162) Pidko, E. A.; Hensen, E. J. M.; Van Santen, R. A. *Proc. R. Soc. London, Ser. A* **2012**, *468*, 2070−2086.
(163) Cundy, C. S.; Cox, P. A. *Chem. Rev.* **2003**, *103*, 663−702.
(164) Cundy, C. S.; Cox, P. A. *Microporous Mesoporous Mater.* **2005**, *82*, 1−78.
(165) Lupulescu, A. I.; Rimer, J. D. *Science* **2014**, *344*, 729−732.
(166) Park, M. B.; Lee, Y.; Zheng, A.; Xiao, F.-S.; Nicholas, C. P.; Lewis, G. J.; Hong, S. B. *J. Am. Chem. Soc.* **2013**, *135*, 2248−2255.
(167) Blackwell, C. S.; Broach, R. W.; Gatter, M. G.; Holmgren, J. S.; Jan, D. Y.; Lewis, G. J.; Mezza, B. J.; Mezza, T. M.; Miller, M. A.; Moscoso, J. G.; et al. *Angew. Chem., Int. Ed.* **2003**, *42*, 1737−1740.
(168) Kim, S. H.; Park, M. B.; Min, H.-K.; Hong, S. B. *Microporous Mesoporous Mater.* **2009**, *123*, 160−168.
(169) Lewis, G. J.; Miller, M. A.; Moscoso, J. G.; Wilson, B. A.; Knight, L. M.; Wilson, S. T. *Stud. Surf. Sci. Catal.* **2004**, *154*, 364−372.
(170) Miller, M. A.; Moscoso, J. G.; Koster, S. C.; Gatter, M. G.; Lewis, G. J. *Stud. Surf. Sci. Catal.* **2007**, *170*, 347−354.
(171) Pinar, A. B.; Gomez-Hortiguela, L.; Perez-Pariente, J. *Chem. Mater.* **2007**, *19*, 5617−5626.
(172) Liu, X.; Luo, Q. *J. Phys. Chem. C* **2017**, *121*, 13211−13217.
(173) Gallego, E. M.; Portilla, M. T.; Paris, C.; León-Escamilla, A.; Boronat, M.; Moliner, M.; Corma, A. *Science* **2017**, *355*, 1051−1054.

DOI: 10.1021/acscatal.7b03676
ACS Catal. 2018, 8, 770−784

(174) Pophale, R.; Daeyaert, F.; Deem, M. W. *J. Mater. Chem. A* **2013**, *1*, 6750−6760.
(175) Schmidt, J. E.; Deem, M. W.; Davis, M. E. *Angew. Chem., Int. Ed.* **2014**, *53*, 8372−8374.
(176) Paolucci, C.; Parekh, A. A.; Khurana, I.; Di Iorio, J. R.; Li, H.; Albarracin Caballero, J. D.; Shih, A. J.; Anggara, T.; Delgass, W. N.; Miller, J. T.; Ribeiro, F. H.; Gounder, R.; Schneider, W. F. *J. Am. Chem. Soc.* **2016**, *138*, 6028−6048.
(177) Lemishko, T.; Valencia, S.; Rey, F.; Jiménez-Ruiz, M.; Sastre, G. *J. Phys. Chem. C* **2016**, *120*, 24904−24909.
(178) Smith, L. J.; Davidson, A.; Cheetham, A. K. *Catal. Lett.* **1997**, *49*, 143−146.
(179) Nikbin, N.; Feng, S.; Caratzoulas, S.; Vlachos, D. G. *J. Phys. Chem. C* **2014**, *118*, 24415−24424.

DOI: 10.1021/acscatal.7b03676
ACS Catal. 2018, 8, 770−784